Journal of Molecular Catalysis A: Chemical 349 (2011) 13–19

Contents lists available at SciVerse ScienceDirect

Journal of Molecular Catalysis A: Chemical

journal homepage: www.elsevier.com/locate/molcata

Editor's Choice paper

Enhanced photoelectric catalytic degradation of methylene blue via TiO_2 nanotube arrays hybridized with graphite-like carbon

Yajun Wang[a,b], Jie Lin[a], Ruilong Zong[a], Jun He[b], Yongfa Zhu[a,*]

[a] Department of Chemistry, Tsinghua University, Beijing 100084, China
[b] National Center for Nanoscience and Technology, 11 Zhongguancun Beiyitiao, Beijing 100190, China

ARTICLE INFO

Article history:
Received 17 January 2011
Received in revised form 17 August 2011
Accepted 22 August 2011
Available online 26 August 2011

Keywords:
Photoelectrical catalysis
Graphite-like carbon
TiO_2 nanotube array
Methylene blue

ABSTRACT

Graphite-like carbon modified TiO_2 nanotube array (TNA-G) photocatalysts were synthesized by sucrose graphitization. After the graphite-like carbon hybridization, these photocatalysts showed the enhanced photoelectric catalytic (PEC) activity under ultraviolet irradiation and the obvious PEC degradation activity under visible irradiation ($\lambda > 450$ nm). And the optimum photoresponse was two and three times higher than that of TNA sample under ultraviolet and visible irradiation ($\lambda > 450$ nm) after the Graphite-like carbon hybridization. The total organic carbon results suggested that TNA-G sample could mineralize methylene blue (MB) effectively. The enhancement of PEC activity originated from the synergetic effect between graphite-like carbon layer and TiO_2 nanotube array (TNA), which enhanced charge separation process remarkably. The different degradation mechanisms of MB under ultraviolet and visible ($\lambda > 450$ nm) irradiation were suggested. MB II was dominating reactant via the PEC process and MB I was nondominant degraded via the photocatalytic process under ultraviolet irradiation; while the electric energy played a more important role under visible ($\lambda > 450$ nm) irradiation, MB I and II were degraded at the same time without distinction.

1. Introduction

Photoelectric catalytic (PEC) oxidation of TiO_2 nanotube array (TNA) has been proven to be an efficient method for degrading organic contaminants in aqueous solution [1–4]. Moreover, photocatalysts in an immobilized film form is more practical than that in a powdery form for application. Considering the photochemical reactions mainly take place on the surface of the catalyst, surface modification is one of the most intriguing methods to build the excellent photocatalyst [5]. Surface modification may change the charge, functionality, reactivity of the catalyst surface and enhance its stability. Several attempts have been made to reduce the recombination of photoinduced hole–electron pairs during the photocatalytic reactions by surface modification [6]. Although the modifications of TNA have been reported to enhance its PEC activity, they focused on the aspects of doping [7] or sensitization [8]. Introduction of electronic effect into TiO_2 is another novel method to achieve the effective separation of photoinduced electron–hole pairs [9].

Conjugated π structures molecules such as C_{60}, PANI have been proven to enhance the photocatalytical performances greatly [10–15]. Graphite has a conjugated structure and the combination of graphite and TiO_2 has attracted a great deal of scientific interest due to the amazing electrical, thermal, and optical properties of graphite. But most of the previous studies focused on the properties of doping or sensitization [16–20]. Our group has reported that after graphite-like carbon surface hybridization (not doping), TiO_2 could transfer the photocarrier more effectively [21] and showed excellent heat stability. In this work, the carbon source was changed from glucose to sucrose; a lower graphitization temperature was achieved. To the best of our knowledge, there has been no report regarding the application of the graphite-like carbon surface modified TiO_2 nanotube in the PEC degradation of organic contaminants. In this work, the PEC properties and the enhancement of PEC activity in degrading methylene blue (MB) of graphite-like carbon modified TiO_2 nanotube array (TNA-G) were systematically investigated to reveal the relationship between the graphite-like carbon hybridization and the enhancement of PEC activity. The enhanced PEC activity originated from the synergistic effect between graphite-like carbon layer and TNA. Moreover, the investigation of intermediates showed that there existed different degradation paths of MB under ultraviolet and visible ($\lambda > 450$ nm) irradiation in the PEC process.

2. Experimental

2.1. Materials and preparation

All chemicals were analytical grade reagents and used without further treatment. Electrolyte was freshly prepared from deionized water. After chemical polishing, titanium foil (thickness about

* Corresponding author. Tel.: +86 10 62787601; fax: +86 10 62787601.
E-mail address: zhuyf@mail.tsinghua.edu.cn (Y. Zhu).

1381-1169/$ – see front matter © 2011 Elsevier B.V. All rights reserved.
doi:10.1016/j.molcata.2011.08.020

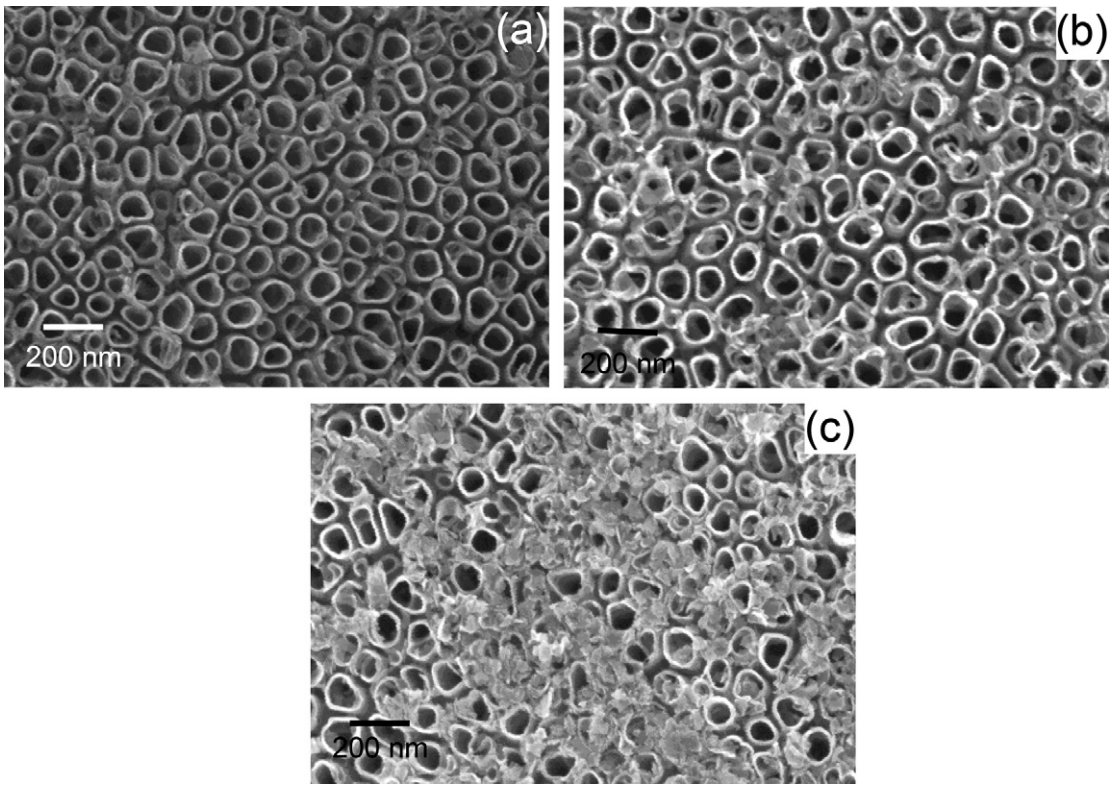

Fig. 1. Morphology of TNA and TNA-G samples at the top view: (a) FESEM image of TNA; (b) FESEM image of TNA-G 0.01 g/mL; (c) FESEM image of TNA-G 0.1 g/mL.

250 μm, purity 99.4%, Beijing Cuibolin Non-Ferrous Technology Developing Co., Ltd.) was subjected to potentiostatic anodization in an electrochemical anodization cell with a platinum cathode in a 0.5 wt% HF + 1 M H_3PO_4 electrolyte at ambient temperature. The potential of 20 V was applied for 30 min. Then the samples were rinsed with deionized water and annealed at 450 °C for 24 h. The TNA-G samples were prepared using sucrose graphitization [18]. The TNA-sucrose precursors were prepared by impregnating TNA film with aqueous solutions of sucrose. Then precursors after drying were calcined at 400 °C in flowing N_2 for 3 h.

2.2. Characterization

The structures of the TNA and TNA-G samples were characterized by XRD (Rigaku D/MAX-2500 X-ray powder diffractometer), using graphite monochromatized Cu Kα radiation (λ = 0.154 nm). A 0.02 step in 2θ/count, beam voltage of 40 kV and beam current of 30 mA were used. The phase composition of the samples was determined by Microscopic Confocal Raman Spectrometer (Renishaw, RM2000) using 632.8 nm as the exciting light source. Spectra were collected in the range of 2000–200 cm^{-1} with a resolution of 1 cm^{-1}. The morphologies and microstructures of the as-prepared samples were observed using a field emission scanning electron microscope (FE-SEM, LEO-1530) at 10 kV and a Tecnai TF20 high-resolution transmission electron microscope (HR-TEM) operated at an accelerating voltage of 200 kV. Ultraviolet–visible diffuse reflectance spectroscopy was performed in Hitachi U-3010, and $BaSO_4$ was used as reference.

2.3. Photoelectric properties and photoelectrocatalytic activities

All electrochemical and photoelectric studies were performed on a CHI660B electrochemical system (Shanghai, China) using a standard three-electrode cell with a working electrode (20 mm × 45 mm), a platinum wire counter electrode, and a saturated calomel electrode (SCE) reference electrode. And 0.1 M Na_2SO_4 was used as electrolyte solution. The electrochemical impedance spectroscopy (EIS) was carried out at the open circuit potential. A sinusoidal ac perturbation of 5 mV was applied to the electrode over the frequency range of 0.05–10^5 Hz. The EIS spectra were further fitted and interpreted by Zsimpwin software. The photoelectric catalytic (PEC) activities of the samples were all evaluated by the removal of MB dye (with an initial concentration of 10 mg/L). UV light was provided by an 18 W germicidal lamp (λ = 254 nm, Institute of Electric Light Source, Beijing). Unless otherwise stated, the intensity of light at the film electrode was 1.64 mW/cm^2 at the wavelength of 254 nm. And visible irradiation was obtained from a 500 W xenon lamp (Institute for Electric Light Sources, Beijing) with a 450 nm cutoff filter and the average visible light intensity was 180 mW/cm^2. The applied bias potential was ranged from 0 V to 6 V. The changes of MB concentration were monitored by the variations in absorption intensity at 660 nm using an ultraviolet–visible spectrometer (Hitachi U-3010). The mineralization of the dye was followed by measuring the total organic carbon (TOC) concentration, utilizing a Shimadzu Corporation TOC-V wp Analyzer.

2.4. Analyses of MB intermediates

To analyze the PEC process of MB, the original concentration of MB was increased to 50 mg/L, and the neutral products were enriched by 140 times. Before the analysis, the samples were filtered through millipore discs of 0.45 μm to protect the chromatographic column. HPLC monitoring was carried out using an ultraviolet absorbance detector (K 2501) operated at 280 nm coupled to a Venusil XBP-C18 (Agela Technologies Inc.) column. The reversed-phase eluent of pH 3 buffer and methanol (45:55, v/v) was used for aqueous solution, and water and methanol (40:60, v/v) were used for enriched neutral products.

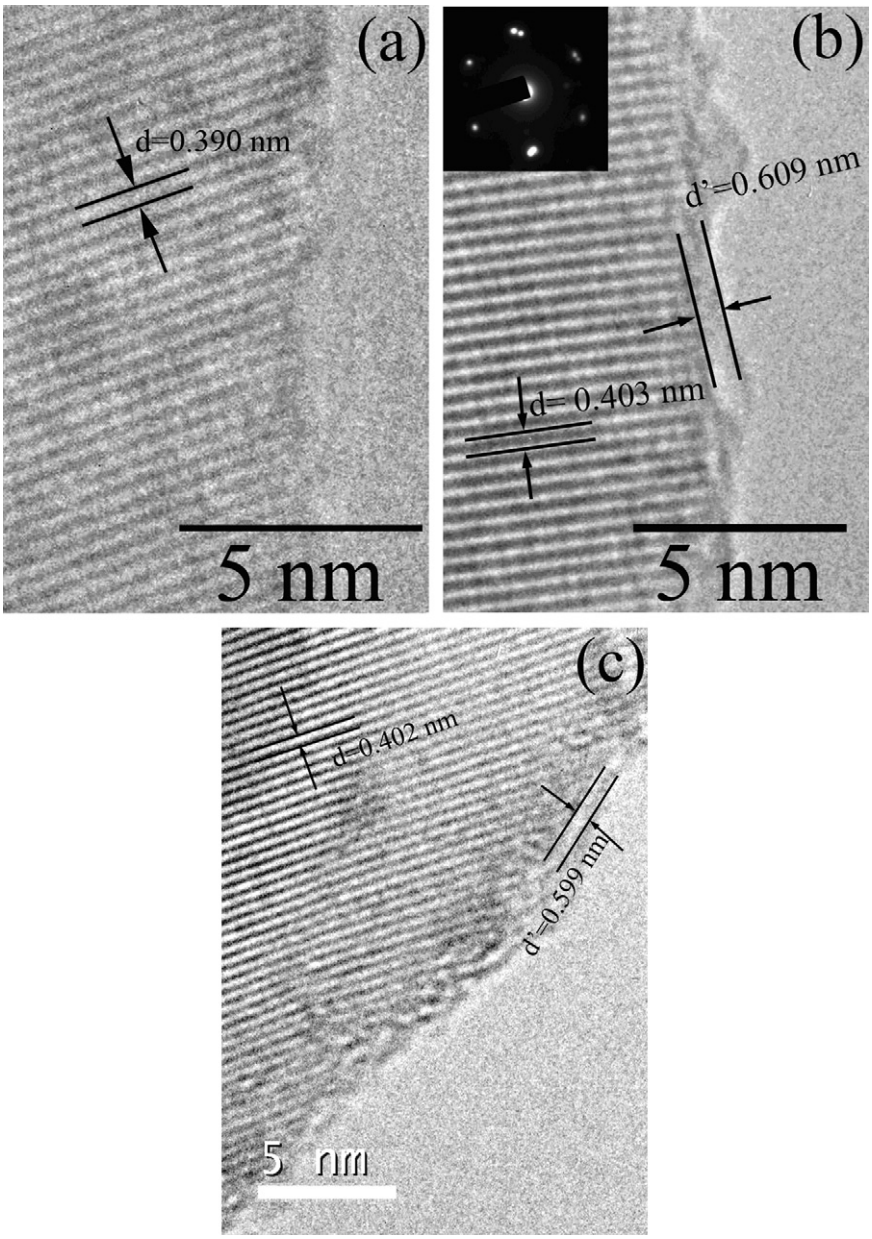

Fig. 2. Morphology of TNA and TNA-G samples: (a) HRTEM image of the TNA sample; (b) HRTEM image of TNA-G 0.01 g/mL, the inset was the selected area electron diffraction (SAED); (c) HRTEM image of TNA-G 0.1 g/mL.

3. Results and discussion

3.1. Structure of TNA-G film

The morphologies of the TNA and TNA-G were obtained by FE-SEM (Fig. 1). The morphology of TNA-G remained the same as that of TNA, and the diameters of TNA film were not changed before and after sucrose graphitization. With increasing the concentration of sucrose, the floccules on the film surface increased. Further study by HR-TEM (Fig. 2) showed that the TNA and TNA-G samples are structurally uniform with a lattice spacing of about 0.400 nm corresponded to the (1 0 1) plane of anatase TiO_2. Although the increase of the sucrose concentration caused the increase of floccules on the film surface, the coverage of nanotube wall was changed little. The thickness of graphite-like carbon layer coated on the TNA-G 0.01 g/mL and TNA-G 0.1 g/mL samples were 0.609 and 0.599 nm, respectively. Since *d*-spacing of graphitic layers was about 0.341 nm, the carbon layer modified on the TiO_2 tube wall was about two graphite layers.

The XRD results (Fig. S1) demonstrated that TiO_2 nanotube held the anatase phase (JCPDS No.: 71-1168) before and after graphite-like carbon modification. In the XRD spectrum of TNA-G 0.01 g/mL sample, the peak of Ti substrate reduced in strength after annealed for the second time, and this phenomenon was not observed in the spectrum of TNA-G 0.1 g/mL. It suggested that annealing could enhance the crystallinity of TiO_2 and the encapsulation of carbon could suppress the crystal growth of TiO_2, which was in agreement with our previous work [21]. The large coverage of carbon on the TNA surface also caused an XRD peak at 27.5° which belonged to the (1 1 1) crystal plane of graphite (JCPDS No.: 75-2078.). The present peak of graphite also illustrated that the carbon on the TNA surface aggregated into crystal, in according with the FE-SEM results. Moreover, peaks related to TiO_xC_y at 36.1° and 61.3° were not be detected in the TNA-G samples, suggesting that carbon was not

doped into the lattice of TiO_2 [22]. In the present work, most of the carbon in the TNA-G samples was free, graphitic carbon.

To confirm the existing form of carbon on the TiO_2 surface, the TNA-G samples prepared with different sucrose concentrations were further characterized by Laser Raman spectroscopy (Fig. S2). The peaks of the TNA and TNA-G samples at 144, 397, 517 and 633 cm^{-1} were belonged to the vibration mode of anatase phase, which confirmed the TiO_2 nanotube array held the anatase phase during the graphite-like carbon modification. In the range of 1200–1800 cm^{-1}, no peak appeared in the TNA-G 0.005 g/mL sample. When the concentration of sucrose increased to 0.01 g/mL, slight peaks at 1360, 1588, 1624 cm^{-1} were observed, which connected with D band, G band and the disorder-induced D′ band of quasi-graphite structure, respectively [23]. The peaks of G band and D′ band which illustrated the fine grain of graphite was obtained in this sample. Moreover, compared with the spectra of pure graphite crystal (1575 cm^{-1}), the G-band shifted to higher wavenumbers in all TNA-G sample spectra, which suggested an intensive chemical interaction between graphite-like carbon and TNA had occurred. The peaks of D band and G band shifted to 1340.5 and 1597.3 cm^{-1} at the TNA-G 0.1 g/mL sample, which was also caused by the size effect [24].

The results above showed that nearly two graphite layers covered TNA sample was formed during the sucrose graphitization process. The thickness of the covered-graphite was not increased with the increase of the sucrose concentration, but the spare graphite covered the TNA surface as floccules. This is likely to be the results of the surface hydrophobic nature of graphite.

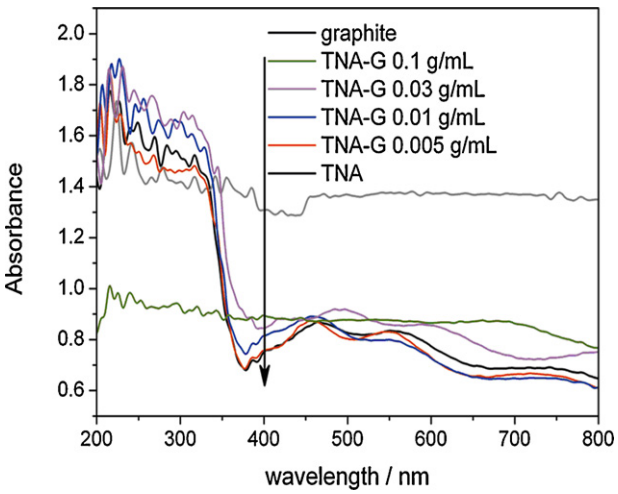

Fig. 3. Diffuse reflectance absorption spectra of TNA, graphite and TNA-G films.

The optical properties of the TNA-G samples were probed with ultraviolet–visible diffuse reflectance spectroscopy (Fig. 3). With increasing the concentration of sucrose, the TNA-G samples kept the absorption character of TiO_2 in the ultraviolet region and extended the absorbance to the visible region due to the presence of graphite-like carbon on the TNA surface. The spectrum of TNA-G

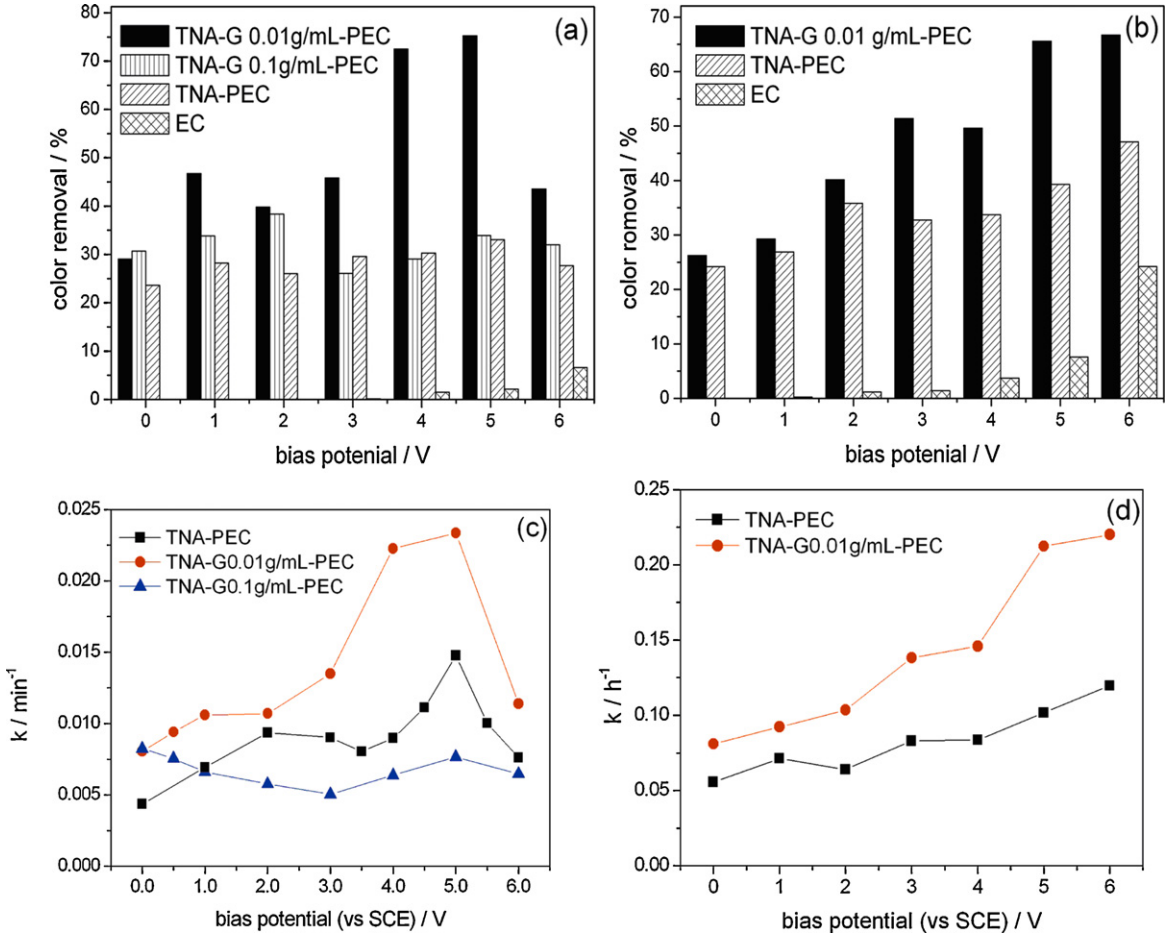

Fig. 4. The catalytic activity of TNA and TNA-G samples: the color removal of MB by the PEC and EC process with TNA and TNA-G samples under ultraviolet for 1 h (a) and visible (λ > 450 nm) irradiation for 5 h (b); the pseudo-first-order kinetic constants of the PEC degradation of MB with TNA and TNA-G samples under ultraviolet irradiation (c) and visible (λ > 450 nm) irradiation (d).

0.1 g/mL sample showed the absorption character of graphite due to the dense coat of graphite on the TNA surface.

3.2. Photoelectrocatalytic degradation activities

The PEC activities of TNA and TNA-G samples were evaluated by the degradation of MB under ultraviolet and visible (λ > 450 nm) irradiation (Fig. 4). The adsorption experiment of TNA-G film and the photolysis were performed as reference. Only 1% of MB was adsorbed on the TNA-G film and 10.2% of MB was removed after 1 h ultraviolet irradiation, so that the adsorption and ultraviolet irradiation did not play the main role on the PEC process. As the electric catalytic (EC) degradation did not obey the pseudo-first-order kinetic, the percent of color removal after reacting under ultraviolet irradiation for 1 h and under visible (λ > 450 nm) irradiation for 5 h were given in Fig. 1. It was seen that 6.58% and 24.21% of MB were removed at 6.0 V after 1 h and 5 h EC degradation. So the EC process was not an effective route to degrade MB. The optimum color removal of the TNA-G 0.01 g/mL sample reached at 5.0 V during the PEC process, which was 2.3 times as that of the pure TNA sample and 35 times as that of the same sample during the EC process. As shown above, the photolysis and EC process were not effective routes to degrade MB, there may be exist a synergetic effect between graphite-like carbon and TNA which was significant to enhance the PEC activity.

Under ultraviolet irradiation, the reaction rate of TNA-G 0.01 g/mL sample increased initially then decreased with the increase of bias, which was similar with our previous study [25]. Comparing with the TNA sample, the activity and MB color removal of TNA-G 0.1 g/mL sample changed less with the bias increasing. This suggested that the multilayered graphite-like carbon did not enhance the PEC activity, namely the conducting coating was not the reason for the enhancement of PEC activity. The PEC activity and MB color removal of TNA-G sample under visible irradiation (λ > 450 nm) increased with the bias increasing, which was similar to the trend of EC process. This result suggested that the electric process played the main role under visible irradiation (λ > 450 nm). When the bias was 6.0 V, the color removal of the TNA-G 0.01 g/mL sample was 1.4 times as that of the TNA sample; while the PEC rate of the TNA-G 0.01 g/mL sample was 1.8 times as that of the TNA sample. Comparing with the PEC process under ultraviolet irradiation, the PEC activity was enhanced less under visible irradiation (λ > 450 nm).

3.3. Mechanism of the enhanced PEC activity

Although the absorption characters of the TNA-G samples were similar with the TNA sample in the ultraviolet region, the photoresponse of the TNA-G samples (Fig. 5a) increased observably. The photoresponse increased with increasing the concentration of sucrose firstly and decreased when the sucrose concentration beyond 0.01 g/mL. The optimum photoresponse was obtained in TNA-G 0.01 g/mL sample, which was twice as high as that of TNA sample at the same condition. A photocurrent spike could be seen when the light was switched on, it was due to the recombination processes of holes which accumulated at the surface and electrons from TiO_2 conduction band [26,27].

Besides under ultraviolet irradiation, the photoresponse of TNA-G sample under visible light (λ > 450 nm) was also enhanced after graphite-like carbon modification (Fig. 5b). Under the bias of 1.0 V, the optimum photoresponse of the TNA-G 0.01 g/mL sample was three times higher than that of TNA sample. Compared with Fig. 5a, a slowly increased photoresponse before the photocurrent reached a steady-state photocurrent could be observed in Fig. 5b. The relatively slow response was due to the photogenerated electrons of TNA-G samples trapped by deep surface state [27].

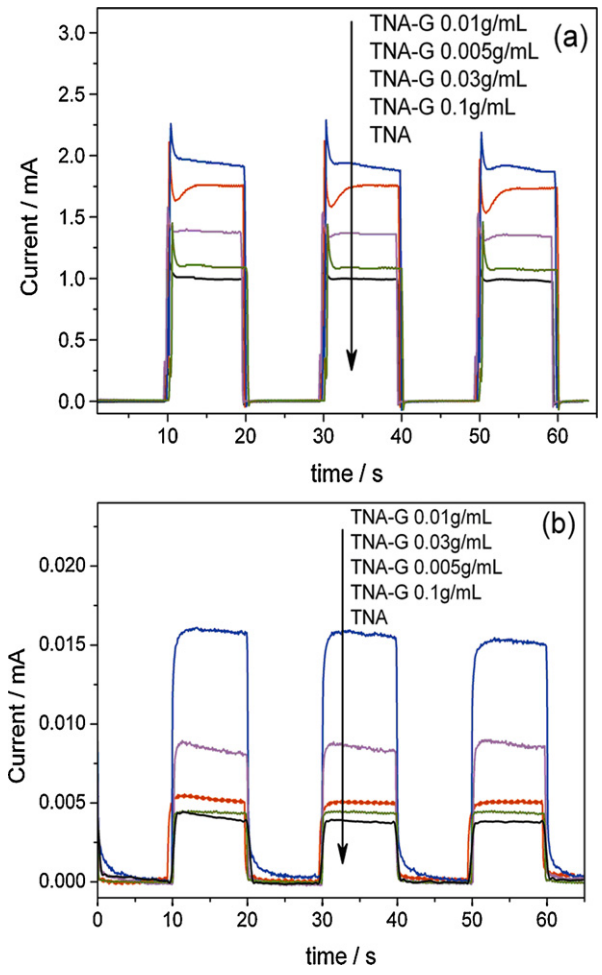

Fig. 5. Photoresponse of the TNA and TNA-G samples: (a) under ultraviolet irradiation; (b) under visible (λ > 450 nm) irradiation with the bias of 1.0 V.

The separation efficiency of photogenerated electrons and holes is a crucial factor for photocatalytic activity. The interface charge separation efficiency can be investigated by EIS (Fig. S3). The EIS plane only showed one semicircle under UV irradiation, which suggested that the charge transfer reaction occurred [28]. The radius of the arc on the EIS spectra reflects the reaction rate occurring at the surface of electrode [29]. Except TNA-G 0.1 g/mL sample, the smaller arc radius on EIS Nynquist plot of TNA-G sample under UV irradiation indicated a more effective separation of photogenerated electron–hole pairs and a faster interfacial charge transfer. To further investigate the influence of graphite-like carbon modification on the photoelectric properties. Equivalent circuits and fitting curves of the TNA-G 0.01 g/mL sample were built in Fig. S3b and c [30]: R_1, solution resistance; R_2, electric charge transfer resistance, corresponding to the Helmholtz layer; R_3, corresponding to the depleting layer; Q, the constant phase elements (CPE) of the inner layer of the TNA-G sample. Using the equivalent circuit, the impedance fitting values were shown in Fig. S3d. The electric charge transfer resistance (R_2) decreased significantly with increasing the sucrose concentration and maintained in equilibrium; while the depleting layer resistance (R_3) decreased firstly then increased gradually. It suggested that the carbon formed on the surface of TNA promote the separation of charges, so that R_2 and R_3 decreased significantly. The coverage of carbon also acted as a light blocking layer, so R_3 increased with increasing the sucrose concentration due to the decrease of photoabsorption.

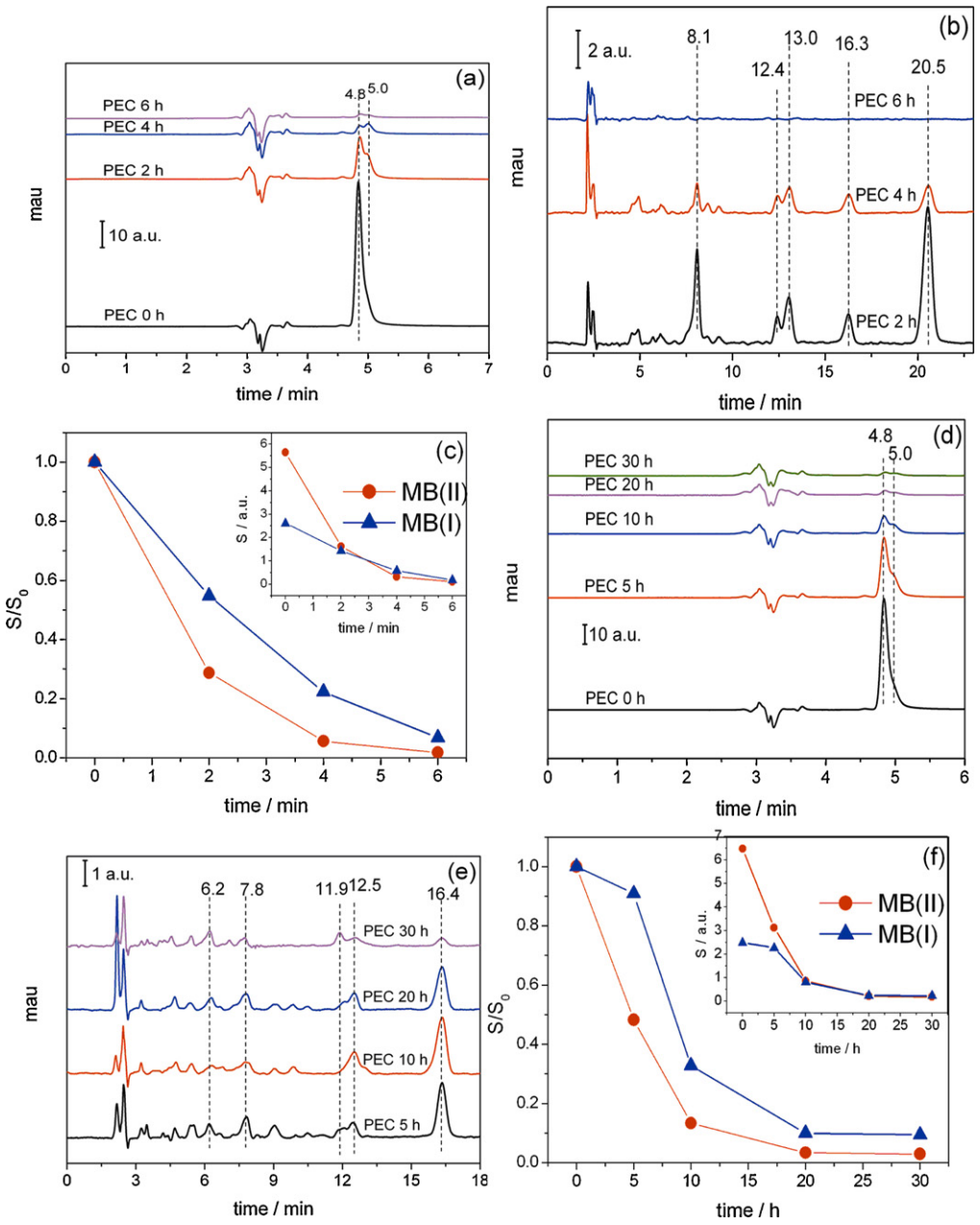

Fig. 6. Chromatograms of MB degradation products in PEC system: (a and d) original solution in methanol–buffer (55:45, v/v) eluent; (b and e) the neutral intermediates enriched by 140 times in methanol–water (60:40, v/v) eluent; (c and f) the change of the relative contentions of MB I and II during the PEC process. (a–c) correspond to the PEC process under ultraviolet irradiation, while (d–f) correspond to that under visible ($\lambda > 450$ nm) irradiation.

The EIS spectra and HR-TEM of TNA-G 0.01 g/mL and 0.1 g/mL samples suggested that the graphite-like carbon coverage formed on the sample surface and nanotube wall played different roles in the PEC property. The two graphite-like carbon layers on the nanotube wall could decrease the depleting and Helmholtz layer resistance and enhance the separation of charges. On the contrary, the graphite floccules mainly acted as a light blocking layer which decreased the photoabsorption. For the thickness of the nanotube wall coverage remained the same and the floccules increased with the increasing sucrose concentration, the charge separation changed little and the photoabsorption was decreased with the sucrose concentration increasing. The competition of enhanced charge separation and decreased photoabsorption caused the TNA-G 0.01 g/mL sample have the optimal PEC activity under UV irradiation.

The EIS spectra of TNA-G samples under visible ($\lambda > 450$ nm) light were also measured. When the covered graphite was thin, the equivalent circuit was similar with that under ultraviolet irradiation; when the covered graphite was thick, the graphite formed a new resistance above the TNA surface. The fitting curves of these two samples (TNA-G 0.01 g/mL and TNA-G 0.1 g/mL) were shown in Fig. S4. It was reported that the graphite-like carbon is able to surface conjugate (d–π conjugate) with the coordinately unsaturated Ti atoms in the surface of TiO_2 to form an optimal structure in previous study [21]. Based on the synergetic effect of graphite-like carbon and TNA, the PEC mechanism of TNA-G under visible light irradiation is proposed as follows: Graphite-like carbon could absorb visible light and the excited state electrons would subsequently inject to the conduction band

(*d*-orbital) of TiO_2 due to the d–π interaction. The excited electrons could react with water and oxygen to generate hydroxyl and superoxide radicals, producing dramatic visible light photocatalytic activity.

3.4. PEC degradation mechanism of MB

To investigate the PEC process of MB, the composition of MB intermediates were detected by HPLC (Fig. 6a and d). Only two peaks were detected from the chromatogram spectra of the original reaction solution. The previous study [31] indicated that two forms of MB existed in the solution (Support Information, Scheme S1), so the two peaks at 4.8 and 5.0 min assigned to MB II and I, respectively. With the analysis of the HPLC results, the relative concentrations of MB I and II were shown in Fig. 6c and f. It was clear that the MB II was degraded more quickly than the MB I under ultraviolet irradiation during the whole PEC process; while the degradation rate of MB II was quicker under visible ($\lambda > 450$ nm) irradiation only at the beginning of the PEC process. These results suggested that the selectivity of MB I and II in the PEC processes under ultraviolet and visible ($\lambda > 450$ nm) irradiation were different. To examine the process in details, the neutral intermediates enriched by 140 times were also detected by HPLC (Fig. 6b and e) and further identified by LC/MS. The suggested structures of the intermediates based on the LC/MS results were similar with our previous study [11] as shown in Supporting Information, Table S1.

Under ultraviolet irradiation, only two peaks at 8.1 and 20.5 min enriched obviously during the PEC process (Fig. 6b). And the two products, 4,6-dichloro-7-dimethylamino-3*H*-S-oxide-phenothiazin-3-one (P1, retention time at 8.1 min) and 3-(5-(dimethylamino)-2-nitrophenylsulfinyl) cyclohexa-2,5-dienone (P2, retention time at 20.1 min), both had a cyclohexa-2,5-dienone structure which was formed through the oxidation of the dimethylamino group. Also the peaks at 12.4, 13.0 and 16.3 min were observed but changed little during the PEC process. These compounds all had the character of oxidation on the N atoms. Combining with the concentration changes of the two MB forms, we suggested that MB II was dominating reactant via the PEC process and MB I was nondominant degraded via the photocatalytic process. The enrichment of P1 and P2 speculated that the rate determinant step occurred at the N atoms, and then the intermediates degraded rapidly.

Different from the PEC process under ultraviolet irradiation, all the peaks of the products changed little under visible ($\lambda > 450$ nm) irradiation. Though the product P2 at 16.4 min was also the main intermediate during the PEC process, the concentration of P2 changed little until the concentration of MB decreased enough. The less concentration of intermediates with S atom oxidation suggested that the effects of photocatalytic process wore off maybe due to less irradiation utilization, namely the electric energy played a more important role at this condition. As the electric effect operated on MB I and II without distinction, MB I and II was degraded at the same time. The fact that the concentration of MB I and II (Fig. 6f) changed similar also validated this point.

The mineralization of dye was also studied by measuring TOC removal (Fig. S5). After PEC process under ultraviolet irradiation for 6 h, the TOC concentration decreased from 2.76 ppm to 0.51 ppm, namely 81.5% of TOC was removed. The TOC concentration change under visible irradiation was similar with the concentration change of MB, namely MB was mineralized completely during the PEC degradation process. These results were consistent with the HPLC results.

4. Conclusion

TNA-G photocatalysts were successfully synthesized by sucrose graphitization, and the synergetic effect between graphite-like carbon and TNA enhanced charge separation process significantly. After introduction of graphite-like carbon, TNA photocatalyst showed the enhanced photoelectric catalytic (PEC) activity under ultraviolet irradiation and the obvious PEC degradation activity under visible irradiation ($\lambda > 450$ nm). TNA-G 0.01 g/mL sample showed the optimal photoelectric response and PEC activity. There existed different mechanisms of MB degradation under ultraviolet and visible light ($\lambda > 450$ nm). MB II was the dominating reactant via the PEC process via the photocatalytic process under ultraviolet irradiation, while MB I and II were degraded at the same time without distinction under visible ($\lambda > 450$ nm) irradiation.

Acknowledgements

This work was partly supported by Chinese National Science Foundation (20673065 and 20925725) and National Basic Research Program of China (2007CB613303).

Appendix A. Supplementary data

Supplementary data associated with this article can be found, in the online version, at doi:10.1016/j.molcata.2011.08.020.

References

[1] Z. Zhang, Yuan, G. Shi, Y. Fang, L. Liang, H. Ding, L. Jin, Environ. Sci. Technol. 41 (2007) 6259–6263.
[2] Y. Xie, L.M. Zhou, H. Huang, Mater. Lett. 60 (2006) 3558–3560.
[3] X. Quan, S. Yang, X. Ruan, H. Zhao, Environ. Sci. Technol. 39 (2005) 3770–3775.
[4] X.M. Wu, Y.H. Ling, J.T. Sun, X. Zhi, Z.H. Huang, Chem. Lett. 37 (2008) 416–417.
[5] H. Noguchi, A. Nakajima, T. Watanabe, K. Hashimoto, Environ. Sci. Technol. 37 (2002) 153–157.
[6] O.V. Makarova, T. Rajh, M.C. Thurnauer, A. Martin, P.A. Kemme, D. Cropek, Environ. Sci. Technol. 34 (2000) 4797–4803.
[7] N. Lu, H. Zhao, J. Li, X. Quan, S. Chen, Sep. Purif. Technol. 62 (2008) 668–673.
[8] W.T. Sun, Y. Yu, H.Y. Pan, X.F. Gao, Q. Chen, L.M. Peng, J. Am. Chem. Soc. 130 (2008) 1124–1125.
[9] H.G. Kim, P.H. Borse, W. Choi, J.S. Lee, Angew. Chem. Int. Ed. 44 (2005) 4585–4589.
[10] H. Zhang, R. Zong, Y. Zhu, J. Phys. Chem. C 113 (2009) 4605–4611.
[11] J. Lin, R. Zong, M. Zhou, Y. Zhu, Appl. Catal. B: Environ. 89 (2009) 425–431.
[12] H. Zhang, R. Zong, J. Zhao, Y. Zhu, Environ. Sci. Technol. 42 (2008) 3803–3807.
[13] H. Fu, T. Xu, S. Zhu, Y. Zhu, Environ. Sci. Technol. 42 (2008) 8064–8069.
[14] S. Zhu, T. Xu, H. Fu, J. Zhao, Y. Zhu, Environ. Sci. Technol. 41 (2007) 6234–6239.
[15] W. Ma, C. Yang, X. Gong, K. Lee, A. Heeger, Adv. Funct. Mater. 15 (2005) 1617–1622.
[16] C. Xu, R. Killmeyer, M.L. Gray, S.U.M. Khan, Appl. Catal. B: Environ. 64 (2006) 312–317.
[17] S. Shanmugam, A. Gabashvili, D.S. Jacob, J.C. Yu, A. Gedanken, Chem. Mater. 18 (2006) 2275–2282.
[18] L. Lin, W. Lin, Y.X. Zhu, B.Y. Zhao, Y.C. Xie, Y. He, Y.F. Zhu, J. Mol. Catal. A: Chem. 236 (2005) 46–53.
[19] S. Sakthivel, H. Kisch, Angew. Chem. Int. Ed. 42 (2003) 4908–4911.
[20] C. Lettmann, K. Hildenbrand, H. Kisch, W. Macyk, W.F. Maier, Appl. Catal. B: Environ. 32 (2001) 215–227.
[21] L.W. Zhang, H.B. Fu, Y.F. Zhu, Adv. Funct. Mater. 18 (2008) 2180–2189.
[22] C. Xu, R. Killmeyer, M.L. Gray, S.U.M. Khan, Electrochem. Commun. 8 (2006) 1650–1654.
[23] L.G. Cançado, A. Jorio, M.A. Pimenta, Phys. Rev. B 76 (2007) 064304.
[24] C. Wen, X. Li, D.Y. Sun, J.Q. Guan, X.X. Liu, Y.R. Lin, S.Y. Tang, G. Zhou, J.D. Lin, Z.H. Jin, Spectrosc. Spectral Anal. 25 (2005) 54–57.
[25] X. Zhao, Y. Zhu, Environ. Sci. Technol. 40 (2006) 3367–3372.
[26] J. Yu, B. Wang, Appl. Catal. B: Environ. 94 (2010) 295–302.
[27] J. Yu, G. Dai, B. Huang, J. Phys. Chem. C 113 (2009) 16394–16401.
[28] J. Li, L. Zheng, L. Li, Y. Xian, L. Jin, J. Hazard. Mater. 139 (2007) 72–78.
[29] W.H. Leng, Z. Zhang, J.Q. Zhang, C.N. Cao, J. Phys. Chem. B 109 (2005) 15008–15023.
[30] W.P. Gomes, D. Vanmaekelbergh, Electrochim. Acta 41 (1996) 967–973.
[31] J.D. Donaldson, S.M. Grimes, N.G. Yasri, B. Wheals, J. Parrick, W.E. Errington, J. Chem. Technol. Biotechnol. 77 (2002) 756–760.